Leader–follower consensus on activity-driven networks

PROCEEDINGS A

rspa.royalsocietypublishing.org

Research

Article submitted to journal

Subject Areas:
applied mathematics, mathematical modelling

Keywords:
consensus, leader-follower, mean-square, network, opinion dynamics, perturbation, time-varying

Author for correspondence:
Alessandro Rizzo
e-mail: alessandro.rizzo@polito.it
Maurizio Porfiri
e-mail: mporfiri@nyu.edu

THE ROYAL SOCIETY PUBLISHING

Leader-follower consensus on activity-driven networks

Jalil Hasanyan[1*], Lorenzo Zino[1*], Daniel Alberto Burbano Lombana[1], Alessandro Rizzo[2,3] and Maurizio Porfiri[1,4]

[1] Department of Mechanical and Aerospace Engineering, New York University Tandon School of Engineering, Brooklyn NY, US
[2]Department of Electronics and Telecommunications, Politecnico di Torino, Turin, Italy
[3]Office of Innovation, New York University Tandon School of Engineering, Brooklyn NY, US
[4] Department of Biomedical Engineering, New York University Tandon School of Engineering, Brooklyn NY, US
∗ These authors contributed equally to the work

Social groups such as schools of fish or flocks of birds display collective dynamics that can be modulated by group leaders, which facilitate decision-making toward a consensus state beneficial to the entire group. For instance, leaders could alert the group about attacking predators or the presence of food sources. Motivated by biological insight on social groups, we examine a stochastic leader-follower consensus problem where information sharing among agents is affected by perceptual constraints and each individual has a different tendency to form social connections. Leveraging tools from stochastic stability and eigenvalue perturbation theories, we study the consensus protocol in a mean-square sense, offering necessary-and-sufficient conditions for asymptotic stability and closed-form estimates of the convergence rate. Surprisingly, the prediction of our minimalistic model share similarities with observed traits of animal and human groups. Specifically, our analysis anticipates the counter-intuitive result that heterogeneity can be beneficial to group decision-making by improving the convergence rate of the consensus protocol. This observation finds support in theoretical and empirical studies on social insects such as spider or honey bee colonies, as well as human teams, where inter-individual variability enhances the group performance.

1. Introduction

Evidence of collective behavior is ubiquitous in animal and human groups [1]. Remarkable examples are flocks of birds or schools of fish, where coordinated maneuvers can enhance protection from predators and optimize energy expenditure [2,3], or the adoption of universal social norms by human groups, where rapid collective cultural shifts determine the emergence on new behaviors that humans are expected to conform to [4,5]. It has been widely observed that a biological advantage is often achieved when group components tend to spontaneously act in unison toward attaining an agreement on a common motion pattern, opinion, or rhythm, relying on local information sharing [1].

Different studies on collective behavior have shown that group decision-making can be strongly influenced by a few members, called *leaders*. These individuals initiate new actions that are readily followed by other group members, called *followers* [6]. Empirical evidence suggests that leadership plays an important role in both animal [7,8] and human coordination [9,10]. Leadership can emerge due to temperament, dominance, or knowledge [11] and might be advantageous to the group. For instance, leaders can provide protection against predatory attacks [12] or knowledge of food sources [13]. Additionally, in situations where the interest and benefit of the majority of group members diverge, leadership can be used to resolve the conflict [14].

The simplest approach to capture decision-making in groups is through consensus protocols [15]. In this class of algorithms, group members (or agents) are modeled as dynamical systems that update their state using information exchanged with others in the group, called *neighbors*, through a communication network [16]. Leadership is typically associated with the tendency of agents to retain their state, rather than compromising with other group members [17]. Followers, on the other hand, update their state through a combination of their own individual dynamics and information exchange from the entire group, including both leaders and followers.

The literature on leader-follower consensus problems is vast, although the majority of existing studies assumes that the communication network among the agents is time-invariant [18–22], or evolves according to a deterministic process [23,24]. Although these modeling schemes have shed light on several features of collective dynamics, they are limited by two restrictive assumptions that might overlook the complexity of human and animal behavior.

First, communication networks are often assumed to emerge according to deterministic rules, whereas stochasticity is known to dominate information exchange in humans and animals [25]. Stochasticity is inherent to the tendency of individuals to share information within the group, such that at a given time an agent in the model should randomly execute the consensus protocol by compromising with randomly selected neighbors. The process of neighbor selection should be constrained by the capacity of individuals to process information, which is encapsulated in the notion of *perceptual numerosity* in biology [26,27] and reverberates in the degree distribution of the communication network of consensus models [12,28,29].

Second, individuals of a group are typically hypothesized to be identical, while they may vastly differ from each other in their behavioral and non-behavioral traits, shaping the process of information sharing in collective dynamics [30]. Within a consensus protocol, heterogeneity within the group should manifest into individual-level variations in the propensity to share information and execute the consensus protocol. For example, the different aerobic capacity of fish determines their positional preference in a school [31], which will challenge individuals in the front of the school to process information from the school and favor changes in the swimming directions of those in rear positions.

Modeling these features calls for advancements in stochastic leader-follower consensus protocols. Recent efforts have been made in this direction. For instance, in [32], the authors examine a consensus protocol where, at each time-step, agents randomly establish a fixed number of connections with a random subset from the group. This notion of a *numerosity-constrained* network is further examined in [33] and [34] to explore more complex collective

dynamics. A treatment of heterogeneity is presented in [35], where the emergence of leadership is studied by weighing differently the communication between agents — restricted to pairwise interactions. While these models partially address some of the limitations of standard practice in the consensus literature, they do not address heterogeneity in the node dynamics within a general communication network.

In this paper, we advance the state of the art of leader-follower consensus problems toward a stochastic framework for information exchange that accounts for numerosity-constraints and individual heterogeneity. We frame our work within the paradigm of activity-driven networks (ADNs) [36,37]. Under the ADN paradigm, the network topology changes according to a stochastic mechanism, whereby each agent sporadically establishes interactions with a fixed number of randomly selected agents in the group. Heterogeneity is modeled through the assignment of an individual parameter, called *activity*, to agents. The activity encapsulates the propensity of each individual to establish links with others. The ADN framework has been successfully employed in different applications, including epidemics [38–40], opinion formation [41,42], diffusion of innovation [43], and percolation problems [44].

ADNs have three main advantages that make them attractive for applications: (i) they are suitable to model the co-evolution of the agents and link dynamics at comparable time scales, avoiding the need of resorting to time-separation assumptions that would lead to approximated (quenched or annealed) representations of the network; (ii) they allow for an elegant and compact representation of agent's heterogeneity through the activity; and (iii) they beget mathematical models that can be analytically tractable and amenable to fast simulations, even for large-scale networks.

Here, we leverage stochastic stability theory [45] and eigenvalue perturbation methods [46] to study leader-follower consensus over ADNs in a mean-square sense. We decompose the analysis in three steps. First, we clarify the relationship between mean-square consensus and the spectral properties of an ancillary matrix, encapsulating second moments of the network evolution. Second, we examine the consensus protocol in the case where all the agents have the same activity. From a technical point of view, the analysis extends the claims of [32], where all the agents are deterministically bound to execute the consensus protocol at each time-step. In the more general case where agents randomly execute the consensus protocol, we establish a closed-form expression for the convergence rate and necessary-and-sufficient conditions for consensus. Finally, we tackle the problem of heterogeneity by applying a perturbation argument that affords a first-order computation of the convergence rate in terms of the heterogeneity in the agents' activities. This perturbation argument complements recent findings on leaderless protocols, where a detrimental effect of heterogeneity was discovered through a second-order analysis [47].

Beyond assisting in the quantification of the role of several model parameters on the consensus dynamics, our minimalistic model of collective behavior is successful in anticipating an adaptative feature of living in groups. Specifically, our theoretical analysis predicts the counter-intuitive result that heterogeneity can be beneficial to group decision-making by improving the convergence rate of the consensus protocol. Heterogeneity among individuals has been shown to be a key factor to improve performance in different biological systems. Several studies indicate that spider colonies with different phenotypes outperform homogeneous colonies in terms of nest defense, foraging, or parental care [48–50]. Behavioral variability conferred by genetic diversity has been shown to enhance the productivity and fitness in honey bee colonies [51]. Beyond social insects, several studies on human teams point at a critical role of heterogeneity on group performance, from the top management in banks [52] to industrial firms [53].

The rest of the paper is organized as follows. In Section 2, the model formulation and the mathematical preliminaries are presented. Our main mathematical results are detailed in Section 3. In Section 4, we discuss our findings by analyzing the role of model parameters on the consensus dynamics. Section 5 concludes the paper and identifies avenues of future research.

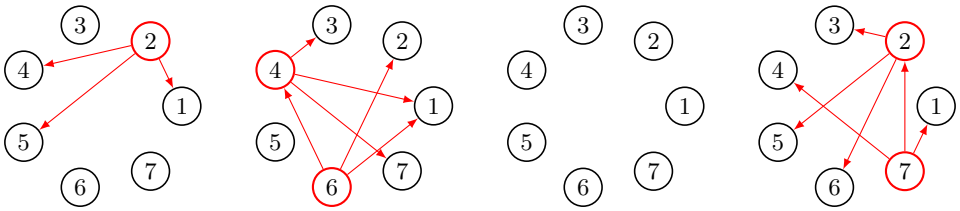

(a) $k=0$ (b) $k=1$ (c) $k=2$ (d) $k=3$

Figure 1: Evolution of an ADN with $n=7$ nodes and $m=3$ over four discrete time-steps. At each time-step, nodes that are active and generate links are colored in red. We observe that the network is generally disconnected and that, at some time-steps, no interaction may be generated (in this realization, for $k=2$).

2. Mathematical preliminaries

(a) Model

We consider a network of $n \geq 4$ agents labeled by positive integers $\mathcal{N} = \{1, \dots, n\}$. Agents belong to two different classes: $f \geq 3$ of them are *followers*, the other $\ell = n - f$, with $\ell \geq 1$, are *leaders*. Without loss of generality, we order agents depending on their class, and we denote by $\mathcal{F} := \{1, \dots, f\}$ and $\mathcal{L} := \{f+1, \dots, n\}$ the sets of followers and leaders, respectively. Each agent is represented by a node of a time-varying network $\mathcal{G}_k = (\mathcal{N}, \mathcal{E}_k)$, where $\mathcal{N}$ is the node set, $\mathcal{E}_k$ is the time-varying edge set, and $k \in \mathbb{Z}^+$ is the nonnegative discrete time index.

The network $\mathcal{G}_k$ evolves according to a discrete-time directed ADN [36]. Specifically, each node $i \in \mathcal{N}$ is assigned an *activity* , $a_i \in (0, 1]$, that is the probability that node i is *active* at each discrete time-step. Activities are gathered into the activity vector $\mathbf{a} \in (0, 1]^n$. An active node generates $m \geq 1$ directed links towards m other nodes, selected uniformly at random among the other $n-1$ nodes. At each iteration, the time index k is updated, connections created in the previous time-step are removed, and a new set of connections is established, independent of previous steps. An example of four consecutive time-steps of an ADN is illustrated in Fig. 1.

At time-step k, the pattern of nodes' interactions is described by the adjacency matrix $A_k \in \{0, 1\}^{n \times n}$ and the graph Laplacian $L_k \in \{-1, 0, m\}^{n \times n}$ [54]. The adjacency matrix is defined as

$$(A_k)_{ij} = \begin{cases} 1 & \text{if } (i,j) \in \mathcal{E}_k \\ 0 & \text{otherwise,} \end{cases} \tag{2.1}$$

and the Laplacian is $L_k := \operatorname{diag}(A_k \mathbf{1}) - A_k$, where $\operatorname{diag}(\cdot)$ is the vector-to-diagonal matrix operator and $\mathbf{1}$ is the vector of all ones[1], that is,

$$(L_k)_{ij} = \begin{cases} -(A_k)_{ij} & \text{if } i \neq j, \\ \sum_{k \in \mathcal{N} \setminus \{i\}} (A_k)_{ik} & \text{if } i = j, \end{cases} = \begin{cases} m & \text{if } i = j,\ i \text{ active at time } k, \\ -1 & \text{if } (i,j) \in \mathcal{E}_k, \\ 0 & \text{otherwise.} \end{cases} \tag{2.2}$$

By construction, matrices L_k's constitute a sequence of independent and identically distributed (IID) random variables with common random variable L.

Each node is associated with a continuous state variable. Nodes' states are stacked in a vector $\mathbf{x}_k \in \mathbb{R}^n$, which represents the overall state of the system at time k. We denote by $\mathbf{y}_k \in \mathbb{R}^f$ and $\mathbf{z}_k \in \mathbb{R}^\ell$ the subvectors gathering the states of followers and of leaders at time k, respectively, so that $\mathbf{x}_k = [\mathbf{y}_k^T \mathbf{z}_k^T]^T \in \mathbb{R}^n$, where superscript T indicates matrix transposition. At each time-step,

[1] Vector and matrix dimensions are usually omitted when they are clear from the context. Only when needed, they will be indicated through subscripts. Subscript k always indicates the discrete time index.

each follower may activate and consequently update its state by performing a weighted average, using a weight $\varepsilon > 0$, with respect to the states of all its neighboring nodes. Parameter ε, called *averaging parameter*, quantifies the willingness of a follower to compromise with its neighbors: the larger ε is, the higher is the influence of the neighbors.

Followers that do not activate at a given time-step maintain their previous state values. Leaders, on the other hand, are assigned a common initial state, $\mathbf{z}_0 = s\mathbf{1}_\ell$, $s \in \mathbb{R}$, which is not changed through iterations. Hence, the network evolves according to

$$\mathbf{x}_{k+1} = (I - \mathcal{E}L_k)\mathbf{x}_k, \tag{2.3}$$

with initial conditions $\mathbf{x}_0 = [\mathbf{y}_0^T \quad s\mathbf{1}_\ell^T]$, where $\mathbf{y}_0$ encodes the arbitrary initial conditions of the followers, I is the identity matrix and $\mathcal{E} = \mathrm{diag}\,([\varepsilon\mathbf{1}_f^T \quad 0\mathbf{1}_\ell^T]^T)$. We refer to the dynamics in (2.3) as the ADN-leader-follower (ADN-LF) consensus protocol.

(b) Problem formulation and mathematical background

The ADN-LF consensus protocol (2.3) can be detailed in terms of leader and follower subsystems. The first f rows of matrix L_k, which are associated with the evolution of the followers' state, can be expressed block-wise as $[\widehat{L}_k \widehat{K}_k] \in \mathbb{R}^{f\times n}$, where $\widehat{L}_k \in \mathbb{R}^{f\times f}$ and $\widehat{K}_k \in \mathbb{R}^{f\times \ell}$. By construction, also the sequences of matrices $\widehat{L}_k$'s and $\widehat{K}_k$'s consist of IID random variables, with common random variables $\widehat{L}$ and $\widehat{K}$, respectively. Therefore, the f-dimensional follower subsystem evolves according to

$$\mathbf{y}_{k+1} = (I - \varepsilon\widehat{L}_k)\mathbf{y}_k - \varepsilon s\widehat{K}_k\mathbf{1}. \tag{2.4}$$

To study the convergence of the ADN-LF consensus protocol in (2.3), we define the disagreement vector, $\boldsymbol{\xi}_k \in \mathbb{R}^f$, as the difference between the states of the followers and that of the leaders, that is, $\boldsymbol{\xi}_k = \mathbf{y}_k - s\mathbf{1}$, following the standard practice of leader-follower consensus protocols [32].

From (2.4), we derive the equation that governs the disagreement dynamics as

$$\boldsymbol{\xi}_{k+1} = (I - \varepsilon\widehat{L}_k)\boldsymbol{\xi}_k, \tag{2.5}$$

with initial condition $\boldsymbol{\xi}_0 = \mathbf{y}_0 - s\mathbf{1}$. The formulation in terms of disagreement dynamics provides a framework to study the consentability of the ADN-LF consensus protocol, by leveraging the following definitions and results [32,55–59].

Definition 2.1 (Definition 1 from [55]). *The ADN-LF consensus protocol in* (2.3) *is said to be mean-square consentable if the disagreement dynamics in* (2.5) *is asymptotically mean-square stable, that is,* $\lim_{k\to\infty} \mathbb{E}[||\boldsymbol{\xi}_k||^2] = 0$, *with* $\mathbb{E}[\cdot]$ *indicating expected value, for all initial conditions* $\boldsymbol{\xi}_0 \in \mathbb{R}^f$.

We observe that, for a jump linear system governed by IID random state matrices like (2.5), mean-square implies almost-sure stability [56,57]. In order to quantify the rate of convergence to consensus, we introduce the asymptotic convergence factor, similar to [59]. This quantity measures the rate of decay of the expectation of the norm of the disagreement dynamics toward zero.

Definition 2.2 (Definition 3 from [59]). *The asymptotic convergence factor, in the mean-square sense, of* (2.5) *is defined as*

$$r := \sup_{||\boldsymbol{\xi}_0||\neq 0} \lim_{k\to\infty} \left(\frac{\mathbb{E}[||\boldsymbol{\xi}_k||^2]}{||\boldsymbol{\xi}_0||^2}\right)^{1/k}. \tag{2.6}$$

We note that the definition of the asymptotic convergence factor is the same in the absence or presence of leaders: the only difference is in the definition of the disagreement dynamics. For the standard consensus protocol, the disagreement is measured with respect to the arithmetic mean of the group, while for leader-follower consensus, it is defined with respect to the state of the leaders.

Using the iterative process in (2.5), the expected value of the squared norm of the disagreement vector can be written as

$$\mathbb{E}[||\boldsymbol{\xi}_k||^2] = \mathrm{vec}(I)^T \mathrm{vec}(\mathbb{E}[\boldsymbol{\xi}_k \boldsymbol{\xi}_k^T]) = \mathrm{vec}(I)^T H^k \mathrm{vec}(\boldsymbol{\xi}_0 \boldsymbol{\xi}_0^T), \tag{2.7}$$

where $\mathrm{vec}(\cdot)$ is the matrix vectorization operator, $H \in \mathbb{R}^{f^2 \times f^2}$ is the second moment matrix of the consensus protocol [32,55], defined as

$$H := \mathbb{E}[(I - \varepsilon \widehat{L}) \otimes (I - \varepsilon \widehat{L})], \tag{2.8}$$

and $\otimes$ is the Kronecker product. The asymptotic convergence factor r in (2.6) can be expressed in terms of the spectral properties of the second moment matrix (2.8) through the following result, whose proof can be found in [55].

Proposition 2.1 (Theorem 1 from [55]). *The asymptotic convergence factor of the ADN-LF consensus protocol (2.3) is equal to the spectral radius of the second moment matrix H, that is, $r = \rho(H)$. Furthermore, consensus protocol in (2.3) is mean-square consentable if and only if the asymptotic convergence factor $r = \rho(H) < 1$.*

This result relates mean-square consentability of a consensus protocol with the second moment matrix H, whose spectral radius regulates the consentability and the speed of convergence of the consensus protocol. Hence, in what follows, most of our effort focuses on the spectral analysis of H.

3. Main findings

Here, we present the computation of the second moment matrix H for the ADN-LF consensus protocol, which allows for the investigation of the consentability and the rate of convergence of the protocol, in light of Proposition 2.1.

Proposition 3.1. *Consider the ADN-LF consensus protocol (2.3). Then, for $f \geq 3$, $\ell \geq 1$, $\varepsilon > 0$, $m \geq 1$, and $a_i \in (0, 1]$, $\forall\, i \in \mathcal{N}$, the diagonal $H^{ii} \in \mathbb{R}^{f \times f}$ and off-diagonal $H^{ij} \in \mathbb{R}^{f \times f}$ blocks of the second moment matrix are given by*

$$\begin{aligned}
H^{ii} &= \Big(q - q^2(n-1)a_i\Big)\Big(\boldsymbol{a}\mathbf{1}^T - a_i \boldsymbol{e}_i \mathbf{1}^T - \mathrm{diag}\,(\boldsymbol{a}) + a_i \boldsymbol{e}_i \boldsymbol{e}_i^T\Big) \\
&\quad + \Big(1 - 2q(n-1)a_i + q^2(n-1)^2 a_i\Big)\boldsymbol{e}_i \mathbf{1}^T + \Big(q - q^2\Big) a_i \Big(\boldsymbol{e}_i \mathbf{1}^T - \boldsymbol{e}_i \boldsymbol{e}_i^T\Big) \\
&\quad - \Big(q(n-1) - q^2(n-1)^2 a_i\Big)\Big(\mathrm{diag}\,(\boldsymbol{a}) - a_i \boldsymbol{e}_i \boldsymbol{e}_i^T\Big) \\
&\quad + \Big(1 - q(n-1)a_i\Big)\Big(I - \boldsymbol{e}_i \boldsymbol{e}_i^T\Big), \\
H^{ij} &= q^2 a_i \Big(\boldsymbol{a}\mathbf{1}^T - a_i \boldsymbol{e}_i \mathbf{1}^T - \mathrm{diag}\,(\boldsymbol{a}) + a_i \boldsymbol{e}_i \boldsymbol{e}_i^T\Big) + \Big(q - q^2(n-1)\Big) a_i \boldsymbol{e}_i \boldsymbol{e}_i^T \\
&\quad + \varepsilon q a_i \boldsymbol{e}_i \boldsymbol{e}_j^T + q \frac{\varepsilon(m-1)}{n-2} a_i \boldsymbol{e}_i (\mathbf{1} - \boldsymbol{e}_i - \boldsymbol{e}_j)^T + q a_i \Big(I - \boldsymbol{e}_i \boldsymbol{e}_i^T\Big) \\
&\quad - q(n-1) a_i \Big(\mathrm{diag}\,(\boldsymbol{a}) - a_i \boldsymbol{e}_i \boldsymbol{e}_i^T\Big),
\end{aligned} \tag{3.1}$$

respectively, where $q = \varepsilon m/(n-1)$, $\boldsymbol{a}$ is the vector gathering all the activities, $\boldsymbol{e}_i$ is the ith vector of the standard basis of $\mathbb{R}^n$.

Proof. The second moment matrix in (2.8) can be expanded as follows:

$$H = I_{f^2} - \varepsilon(\mathbb{E}[\widehat{L}] \oplus \mathbb{E}[\widehat{L}]) + \varepsilon^2 \mathbb{E}[\widehat{L} \otimes \widehat{L}], \tag{3.2}$$

where $\oplus$ is the Kronecker sum. We compute $\mathbb{E}[\widehat{L}]$ by observing that the diagonal entries of matrix $\widehat{L}$ are either equal to m or 0. In particular, the probability $P(L_{ii} = m) = a_i$, for all $i \in \mathcal{F}$. The off-diagonal terms are either equal to -1 or 0. Thus, $P(L_{ij} = -1) = \dfrac{ma_i}{n-1}$, for all i and $j \neq i$. Hence, it holds

$$\mathbb{E}[\widehat{L}] = \frac{n}{n-1} m \operatorname{diag}(\mathbf{a}) \left(I - \frac{1}{n} \mathbf{1}\mathbf{1}^T \right). \tag{3.3}$$

We compute $\mathbb{E}[\widehat{L} \otimes \widehat{L}]$, by leveraging the block structure of $\widehat{L}$ and the definition of the Kronecker product. Specifically, we write general entries in the form $\mathbb{E}[\widehat{L} \otimes \widehat{L}]^{jh}_{ip} = \mathbb{E}[\widehat{L}_{ip} \widehat{L}_{jh}]$, for $i, j, h, p \in \mathcal{F}$. The ADN-LF consensus protocol begets a regularity in the structure of $\mathbb{E}[\widehat{L} \otimes \widehat{L}]$, which is encoded by only seven distinct cases. The structure of the generally nonsymmetric matrix $\mathbb{E}[\widehat{L} \otimes \widehat{L}]$ can be represented through the following cases: (c_1) $i = j = p = h$; (c_2) $i \neq j, i = k, j = h$; (c_3) $i = j = h$ and $j \neq p$, or $i = j = p$ and $j \neq h$; (c_4) $i \neq j, i \neq p$, and $j = h$, or $i = p, i \neq j, j \neq h$; (c_5) $i = j, i \neq p, h = p$; (c_6) $i = j, i \neq h, i \neq p, h \neq p$; and (c_7) $i \neq j, i \neq p, j \neq h$, as follows:

$$E[\widehat{L} \otimes \widehat{L}] = \left[\begin{array}{cccc|cccc|ccc|c}
c_1 & c_3 & \cdots & c_3 & c_3 & c_5 & \cdots & c_6 & \cdots & c_3 & c_6 & \cdots & c_5 \\
c_4 & c_2 & \cdots & c_4 & c_7 & c_4 & \cdots & c_7 & \cdots & c_7 & c_4 & \cdots & c_7 \\
\vdots & \vdots & \ddots & \vdots & \vdots & \vdots & \ddots & \vdots & \ddots & \vdots & \vdots & \ddots & \vdots \\
c_4 & c_4 & \cdots & c_2 & c_7 & c_7 & \cdots & c_4 & \cdots & c_7 & c_7 & \cdots & c_4 \\
\hline
c_4 & c_7 & \cdots & c_7 & c_2 & c_4 & \cdots & c_4 & \cdots & c_4 & c_7 & \cdots & c_7 \\
c_5 & c_3 & \cdots & c_6 & c_3 & c_1 & \cdots & c_3 & \cdots & c_6 & c_3 & \cdots & c_5 \\
\vdots & \vdots & \ddots & \vdots & \vdots & \vdots & \ddots & \vdots & \ddots & \vdots & \vdots & \ddots & \vdots \\
c_7 & c_7 & \cdots & c_4 & c_4 & c_4 & \cdots & c_2 & \cdots & c_7 & c_7 & \cdots & c_4 \\
\hline
\vdots & \vdots & \ddots & \vdots & \vdots & \vdots & \ddots & \vdots & \ddots & \vdots & \vdots & \ddots & \vdots \\
\hline
c_4 & c_7 & \cdots & c_7 & c_4 & c_7 & \cdots & c_7 & \cdots & c_2 & c_4 & \cdots & c_4 \\
c_7 & c_4 & \cdots & c_7 & c_7 & c_4 & \cdots & c_7 & \cdots & c_4 & c_2 & \cdots & c_4 \\
\vdots & \vdots & \ddots & \vdots & \vdots & \vdots & \ddots & \vdots & \ddots & \vdots & \vdots & \ddots & \vdots \\
c_5 & c_6 & \cdots & c_3 & c_6 & c_5 & \cdots & c_3 & \cdots & c_3 & c_3 & \cdots & c_1
\end{array}\right]. \tag{3.4}$$

The observations on the structure of matrix $\widehat{L}$ made above, the stochastic independence between its rows, and a counting argument on the Kronecker product lead to the following seven entries: $c_1 = \mathbb{E}[\widehat{L} \otimes \widehat{L}]^{ii}_{ii} = m^2 a_i$; $c_2 = \mathbb{E}[\widehat{L} \otimes \widehat{L}]^{jj}_{ii} = m^2 a_i a_j$; $c_3 = \mathbb{E}[\widehat{L} \otimes \widehat{L}]^{jj}_{jp} = \mathbb{E}[\widehat{L} \otimes \widehat{L}]^{jh}_{jj} = -ma_j/(n-1)$; $c_4 = \mathbb{E}[\widehat{L} \otimes \widehat{L}]^{jj}_{ip} = \mathbb{E}[\widehat{L} \otimes \widehat{L}]^{jh}_{ii} = -m^2 a_i a_j/(n-1)$; $c_5 = \mathbb{E}[\widehat{L} \otimes \widehat{L}]^{ip}_{ip} = ma_i/(n-1)$; $c_6 = \mathbb{E}[\widehat{L} \otimes \widehat{L}]^{ih}_{ip} = m(m-1)a_i/(n-1)(n-2)$; and $c_7 = \mathbb{E}[\widehat{L} \otimes \widehat{L}]^{jh}_{ip} = m^2 a_i a_j/(n-1)^2$. □

Remark 3.1. *By analyzing the seven entries of $\mathbb{E}[\widehat{L} \otimes \widehat{L}]$, we identify several features. The constants c_2, c_4, and c_7, formed by elements pertaining to different rows of the block and different rows within the block, are proportional to the two activities of the agents corresponding to the matrix entries. The other constants refer to elements sharing the same row of the block and the same row within the block; these entries are proportional to the activity of the corresponding agent. Notably, entry c_6 reflects the effect of the numerosity constraint.*

Remark 3.2. *We note that the expression in Proposition 3.1 does not reduce to the second moment matrix of the leader-follower consensus protocol over a numerosity-constrained network [32] unless $\mathbf{a} = \mathbf{1}$. If all the activities are equal but they are different from 1, the ADN-LF consensus protocol does not correspond to the consensus protocol over a numerosity-constrained network, due to the nonlinear influence of the activities*

on H. Consequently, the effect of the stochastic activation mechanism is not a mere temporal scaling of the process, which is further exacerbated for the general case of heterogeneous activities.

The complexity of the general structure of H, demonstrated in Proposition 3.1, challenges the development of general closed-form results. For the specific case of homogeneous activities, yielding a simplified form of H, we can compute eigenvalues and eigenvectors in closed-form, as shown in Section 3(a). Expanding to heterogeneous activities, we can pursue a perturbation argument with respect to the homogeneous case, as detailed in Section 3(b).

(a) Homogeneous case

We consider an ADN with a homogeneous vector of activities, that is, $a_i = a \in (0,1]$, for all $i \in \mathcal{N}$. Then, the second moment matrix H in Proposition 3.1 simplifies to matrix H_0 as

$$\begin{aligned}
(H_0)^{ii} &= qa\Big(1-q(n-1)a\Big)\mathbf{1}\mathbf{1}^T + q^2a(n-1)(a-1)\mathbf{e}_i\mathbf{1}^T \\
&\quad + \Big(1-qa(2n-1)+q^2a^2n(n-1)\Big)I + q^2n(n-1)a(1-a)\mathbf{e}_i\mathbf{e}_i^T, \\
(H_0)^{ij} &= q^2a^2\mathbf{1}\mathbf{1}^T + qa\left(\varepsilon\frac{m-1}{n-2}-qa\right)\mathbf{e}_i\mathbf{1}^T + qa(1-qna)I \\
&\quad + qa\left(qna-q(n-1)-\varepsilon\frac{m-1}{n-2}\right)\mathbf{e}_i\mathbf{e}_i^T + \varepsilon qa\left(1-\frac{m-1}{n-2}\right)\mathbf{e}_i\mathbf{e}_j^T,
\end{aligned} \tag{3.5}$$

where $q = \varepsilon m/(n-1)$. The eigenvalues and eigenvectors of H_0 can be analytically computed as detailed in the following proposition; the proof is reported in the Appendix.

Proposition 3.2. *Consider the ADN-LF consensus protocol (2.3). Then, for $f \geq 3$, $\ell \geq 1$, $\varepsilon > 0$, $m \geq 1$, and $a_i = a \in (0,1]$, $\forall\, i \in \mathcal{N}$, the second moment matrix H_0 has eigenvectors of the form $\boldsymbol{v} = [\boldsymbol{v}_1^T \dots \boldsymbol{v}_f^T]^T$, with $\boldsymbol{v}_i \in \mathbb{R}^f$, $i \in \mathcal{F}$, belonging to eigenspaces $\Gamma_1, \dots, \Gamma_6$, defined by*

$$\begin{aligned}
\Gamma_1 &= \left\{\boldsymbol{v}\in\mathbb{R}^{f^2} : \sum_{i\in\mathcal{F}}\boldsymbol{v}_i = 0,\ \boldsymbol{v}_i^T\mathbf{1}=0,\quad \boldsymbol{e}_i^T\boldsymbol{v}_i = 0,\quad i\in\mathcal{F}\right\}, \\
\Gamma_2 &= \left\{\boldsymbol{v}\in\mathbb{R}^{f^2} : \boldsymbol{v}_i = -\mu_i\mathbf{1} + \sum_{j\in\mathcal{F}}\mu_j\boldsymbol{e}_j,\quad \mu\in\mathbb{R}^f,\quad \mu^T\mathbf{1}=0,\quad i\in\mathcal{F}\right\}, \\
\Gamma_{3,4} &= \left\{\boldsymbol{v}\in\mathbb{R}^{f^2} : \boldsymbol{v}_i = \mu_i\boldsymbol{e}_i - \frac{1}{\gamma_{3,4}+2}\left(\mu_i\mathbf{1} + \sum_{j\in\mathcal{F}}\mu_j\boldsymbol{e}_j\right),\quad \mu\in\mathbb{R}^f,\quad \mu^T\mathbf{1}=0,\quad i\in\mathcal{F}\right\}, \\
\Gamma_{5,6} &= \left\{\boldsymbol{v}\in\mathbb{R}^{f^2} : \boldsymbol{v}_i = \boldsymbol{e}_i + \gamma_{5,6}\mathbf{1},\quad i\in\mathcal{F}\right\},
\end{aligned} \tag{3.6}$$

with corresponding eigenvalues

$$\begin{aligned}
\lambda_1 &= (1-nqa)^2, \\
\lambda_2 &= 1-qa(n+\ell)+q^2a^2n\ell, \\
\lambda_{3,4} &= (1-nqa)^2 + (nq^2a^2-qa)(\gamma_{3,4}+2-f), \\
\lambda_{5,6} &= (1-\ell qa)^2 + \frac{2qa-(n+\ell)q^2a^2}{\gamma_{5,6}},
\end{aligned} \tag{3.7}$$

where constants $\gamma_3, \dots, \gamma_6$ are reported in the Appendix. The eigenvalues have (geometric) multiplicity equal to f^2-3f+1, $f-1$, $f-1$, $f-1$, 1, and 1, respectively. In addition, all the eigenvalues are real and the matrix is diagonalizable.

Remark 3.3. *Proposition 3.2 highlights the relationship between the eigenstructure of H_0 and model parameters. Apart from its dimension, the structure of Γ_1 is independent from the model parameters, and the corresponding eigenvalue γ_1 is only influenced by ε and the parameters of the ADN (that is, a, n, and*

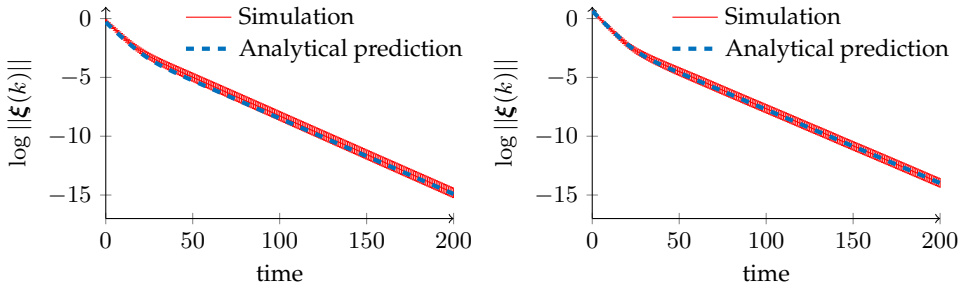

(a) $n = 18,\ f = 12,\ m = 3$ (b) $n = 60\ f = 45,\ m = 4$

Figure 2: Norm of the disagreement vector computed over 200 independent Monte Carlo simulations (red line) and corresponding 99% confidence intervals, compared with our analytical prediction from Theorem 3.1 (blue dashed line), for different parameters settings. In each of the two figures, all the simulations share the same initial conditions, where the initial state for each follower is generated uniformly at random in $[0, 1]$. Common parameters are $\varepsilon = 0.2$ and $\mathbf{a} = a\mathbf{1}$ with $a = 0.3$.

m). The structure of Γ_2 is independent from model parameters, while λ_2 depends on all of them, including the number of leaders ℓ. The other four pairs of eigenspaces and eigenvectors are influenced by all the model parameters. Following up on Remark 3.2, in the specific case of the homogeneous ADN-LF with $a = 1$, Proposition 3.2 reduces to Proposition 2 in [32].

We use the complete spectral characterization of matrix H_0 to determine its spectral radius and, ultimately, a closed-form expression for the asymptotic convergence factor r defined in (2.6), by using Proposition 2.1. Our results are summarized in the following theorem.

Theorem 3.1. *Consider the ADN-LF consensus protocol (2.3). Then, for $f \geq 3$, $\ell \geq 1$, $\varepsilon > 0$, $m \geq 1$, and $a_i = a \in (0, 1]$, $\forall\, i \in \mathcal{N}$, its asymptotic convergence factor is $r = \lambda_6$, as defined in (3.7).*

Proof. We determine the asymptotic convergence factor by examining the spectral decomposition of H_0, that is, $UHV = \Lambda$, where

$$\Lambda = \text{diag}\left([\lambda_1 \mathbf{1}^T_{f^2-3f+1} \quad \lambda_2 \mathbf{1}^T_{f-1} \quad \lambda_3 \mathbf{1}^T_{f-1} \quad \lambda_4 \mathbf{1}^T_{f-1} \quad \lambda_5 \quad \lambda_6]^T \right). \tag{3.8}$$

Matrix V contains the f^2 linearly independent (right) eigenvectors of H_0, and U contains the left eigenvectors, defined in the Appendix.

Note that $UV = I_{f^2}$, and that the first four left and right eigenspaces of H_0 are orthogonal to $\text{vec}(I)$. Thus, we can express (2.5) as

$$\mathbb{E}[||\boldsymbol{\xi}_k||^2] = \frac{(1+\gamma_5)(||\boldsymbol{\xi}_0||^2 + \omega_5(\boldsymbol{\xi}_0^T \mathbf{1})^2)}{1+\gamma_5+\omega_5+\gamma_5\omega_5}\lambda_5^k + \frac{(1+\gamma_6)(||\boldsymbol{\xi}_0||^2 + \omega_6(\boldsymbol{\xi}_0^T \mathbf{1})^2)}{1+\gamma_6+\omega_6+\gamma_6\omega_6}\lambda_6^k. \tag{3.9}$$

Finally, through standard algebra we compare the two eigenvalues λ_5 and λ_6, and we prove that $|\lambda_6| > |\lambda_5|$, for any admissible choice of the model parameters, which yields the claim. □

In Fig. 2, we compare our analytical predictions of the disagreement dynamics from Theorem 3.1 with their Monte Carlo numerical estimation (computed over 200 independent runs with the same initial condition), in two different parameters settings. In both cases, we observe a satisfactory agreement between the two quantities. In Fig. 2a, the asymptotic convergence factor is analytically computed as $r = 0.8794$, while its numerical estimation, computed through best line fit after a transient of $k = 40$ steps, gives the estimation 0.8776. Similarly, in Fig. 2b, we

analytically predict $r = 0.8814$, against a numerical estimation 0.8814. In both cases, the difference between analytical prediction and numerical estimation is smaller than 0.3%, thereby confirming the validity of our closed-form results.

(b) Heterogeneous case

Next, we consider the case when the activities in the ADN-LF consensus protocol eqrefeq:consensus are nonidentical. The complex structure of the second moment matrix H challenges the analytical study of consentability for this general case. To overcome this issue, we tackle the analysis through a first-order perturbation argument. Toward this aim, we define $\bar{a}$ as the average activity and σ as the standard deviation of the activities, such that

$$\bar{a} := \frac{1}{n}\sum_{i\in\mathcal{N}} a_i, \qquad \sigma := \sqrt{\frac{1}{n}\sum_{i\in\mathcal{N}}(a_i-\bar{a})^2}. \tag{3.10}$$

We observe that the entries of the vector of activities $\mathbf{a}$ can be written as

$$a_i = \bar{a} + \sigma h_i, \tag{3.11}$$

where $h_i \in \mathbb{R}$ measures the deviation of each nodal activity from the average, vector $\mathbf{h}$ is such that $\mathbf{1}^T\mathbf{h} = 0$, and $||\mathbf{h}|| = \sqrt{n}$. Furthermore, we denote the overall deviations of the followers as $\alpha := \sum_{i\in\mathcal{F}} h_i$.

Utilizing (3.11), we can expand the second moment matrix H in (3.1) as

$$H = H_0 + \sigma H_1 + O(\sigma^2), \tag{3.12}$$

where H_0 is the second moment matrix (3.5) for a homogeneous ADN with all activities equal to $\bar{a}$ and H_1 is reported in (A 6) in the Appendix. Perturbation analysis allows for an explicit closed-form expression of the asymptotic convergence factor of the ADN-LF consensus protocol through the following result.

Proposition 3.3 (From [46]). *Consider the second moment matrix H in (3.12). Let ρ_0 be the simple eigenvalue associated with the spectral radius of H_0 and u_0 be its corresponding unit-norm eigenvector. Then, the spectral radius of H is equal to $\rho(H) = \rho_0 + \sigma\rho_1 + O(\sigma^2)$, where $\rho_1 = u_0^T H_1 u_0$ is the first-order eigenvalue perturbation.*

The result of the application of Proposition 3.3 to the second moment matrix H for the ADN-LF consensus protocol (2.3), in the presence of heterogeneity, is reported in the following proposition; details of the proof are provided in the Appendix.

Proposition 3.4. *Consider matrix H in (3.12) with $f \geq 3$, $\ell \geq 1$, $\varepsilon > 0$, $m \geq 1$, and $\bar{a} \in (0, 1]$. The first-order perturbation of the spectral radius of H_0 is*

$$\begin{aligned}\rho_1 \;=\; \alpha\Bigg[&\gamma_6^2\Big(-2q^2\ell^2\bar{a}(f-1) - q\ell f + q^2(n-1)(\ell-f+1) + \varepsilon q(f-1)\\ &+\frac{\varepsilon q(m-1)(f-1)(f-2)}{n-2}\Big) + \gamma_6\Big(2q(\ell f - n - \ell) + 2q^2(n-1)\ell\\ &+\frac{\varepsilon q(m-1)(f-1)(f-2)}{n-2} - 2q^2\bar{a}(n+\ell)(\ell f - 1) + 2(f-1)\varepsilon q\Big) - 2qf\\ &-2q^2\ell\bar{a}(n+\ell)(\ell-1) - 2qf + q^2(n-1)^2 + (f-1)\varepsilon q\Bigg]/(\gamma_6^2 f^2 + 2\gamma_6 f + f),\end{aligned} \tag{3.13}$$

where the constant γ_6 is given in the Appendix upon setting $a = \bar{a}$.

Through the perturbation argument in Proposition 3.3, the asymptotic convergence factor of a general ADN-LF consensus protocol can be expressed in terms of the asymptotic convergence

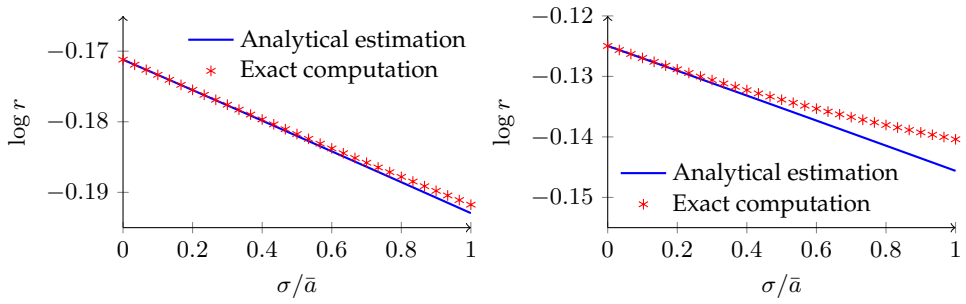

(a) $n = 18,\ f = 12,\ m = 3,\ \alpha = 1.4505$ (b) $n = 60,\ f = 45,\ m = 4,\ \alpha = 7.1223$

Figure 3: Comparison between the first-order perturbation of the asymptotic convergence factor (blue solid line) and the numerical computation of the spectral radius of the exact second moment matrix (red stars), for different levels of heterogeneity and parameters settings. Common parameters are $\varepsilon = 0.2$, $\bar{a} = 0.3$, and the vector $\mathbf{h}$ is generated at random, given α.

factor when all the activities are equal to each other ($a_i = \bar{a},\ \forall\, i \in \mathcal{N}$), computed according to Theorem 3.1, and the first-order perturbation presented in Proposition 3.4. This claim is formalized through the following theorem.

Theorem 3.2. *Consider the ADN-LF consensus protocol* (2.3)*. Then, for* $f \geq 3$, $\ell \geq 1$, $\varepsilon > 0$, $m \geq 1$, *and* $\boldsymbol{a} = \bar{a}\mathbf{1} + \sigma \boldsymbol{h}$, *its asymptotic convergence factor is equal to* $r = \lambda_6 + \sigma\rho_1 + O(\sigma^2)$, *where* λ_6 *is given in* (3.7) *upon setting* $a = \bar{a}$ *and* ρ_1 *is presented in* (3.13)*.*

We observe that the first-order perturbation in (3.13) is proportional to the parameter α, that is, the sum of the followers' activity deviations. Therefore, a sensible choice of the components of vector $\mathbf{h}$ may be used to regulate the rate of convergence of the ADN-LF consensus protocol. In this sense, heterogeneity can be interpreted as a control parameter for the speed at which agents find an agreement. In Fig. 3, we provide evidence of the previous claim, showing an instance in which vector $\mathbf{h}$ is chosen to improve the convergence rate.

The figure also verifies the accuracy of the first-order approximation in the proposed perturbation analysis. We observe a remarkable agreement between predictions through perturbation theory and the numerical computation of asymptotic convergence factor from spectral radius of the complete matrix. Such an agreement extends up to perturbations of the same order of magnitude of the average activity. Finally, we notice that higher-order terms — neglected by the first-order analysis — seem to increase the asymptotic convergence factor, thereby slowing down convergence, similar to observations for the case of leaderless protocols [47]. The precise estimation of these nonlinear terms calls for a higher-order perturbation analysis, which will be part of our future research.

An elegant form of the asymptotic convergence factor in Theorem 3.2 can be derived in the thermodynamic limit of large groups, that is, for $n \to \infty$. We assume that the fraction of followers remains constant as the group grows, that is, we assume $f = \kappa n$ and $\ell = (1 - \kappa)n$, for some $\kappa \in (0, 1)$. Under this assumption, the asymptotic convergence factor tends to the expression detailed in the following corollary.

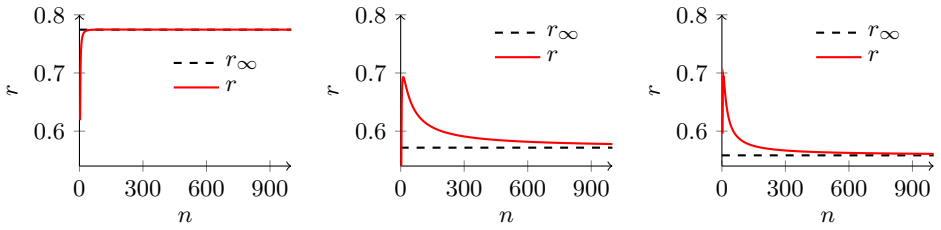

(a) $\varepsilon = 0.2$ (b) $\varepsilon = 0.3$ (c) $\varepsilon = 0.4$

Figure 4: Asymptotic convergence factor for large networks. The black line is r_∞, computed in Corollary 3.1, and the red line is the asymptotic convergence factor computed in Theorem 3.2, for increasing network sizes n. Common parameters are $\kappa = 0.5$, $m = 4$, $\bar{a} = 0.3$, $\sigma = 0.3$, and the vector $\mathbf{h}$ is generated at random such that $\alpha = 1$.

Corollary 3.1. *For $n \to \infty$, the asymptotic convergence factor r of the ADN-LF consensus protocol (2.3) with $\varepsilon > 0$, $\kappa \in (0,1)$, $\boldsymbol{a} = \bar{a}\mathbf{1} + \sigma\boldsymbol{h}$, and $m \geq 1$, approaches*

$$r_\infty = \begin{cases} (1 - \varepsilon m\bar{a}(1-\kappa))^2 & \text{if } \varepsilon \leq \dfrac{2\kappa}{\kappa + m - m\bar{a}(1-\kappa)^2}, \\ 1 - 2\varepsilon m\bar{a} + \varepsilon^2 m\bar{a}(m+\kappa) - 2\sigma\alpha\varepsilon^2 m^2 \bar{a}\dfrac{(1-\kappa)^2(2-\kappa)}{\kappa} & \text{if } \varepsilon > \dfrac{2\kappa}{\kappa + m - m\bar{a}(1-\kappa)^2}. \end{cases} \tag{3.14}$$

Proof. We compute limit expressions for γ_6. If $\varepsilon \leq 2\kappa/(\kappa + m - m\bar{a}(1-\kappa)^2)$, then

$$\lim_{n\to\infty} \frac{\gamma_6}{n} = \frac{\varepsilon m\bar{a}(1-\kappa)^2 + 2\kappa - \varepsilon\kappa - \varepsilon m}{\varepsilon\kappa + \varepsilon(m-1)^2 + \varepsilon m(1-2\kappa) - \varepsilon m\bar{a}(1-\kappa)^2}. \tag{3.15}$$

Otherwise, we find

$$\lim_{n\to\infty} \gamma_6 n = \frac{2 - \varepsilon m\bar{a}(2-\kappa)}{\varepsilon\kappa - 2\kappa + \varepsilon m - \varepsilon m\bar{a}(1-\kappa)^2}. \tag{3.16}$$

The use of either (3.15) or (3.16), and the explicit computation of the limit of λ_6 for $n \to \infty$ yield the claim. □

In the thermodynamic limit of large groups, Corollary 3.1 shows that the effect of heterogeneity increases with ε. The coefficient of α in (3.15) is positive, such that it is always possible to accelerate convergence by introducing heterogeneity in the activities. Predictably, we observe that the favorable effect of heterogeneity increases as the number of leaders in the group and the average activity increase. In Fig. 4, we illustrate the dependence of the asymptotic convergence factor r on the group size for different values of ε. Therein, we also report the limit value r_∞ computed in Corollary 3.1 for large groups, considering three different parameter settings. Overall, we find that the thermodynamic limit accurately represents the asymptotic convergence factor for groups of more than 100 agents.

4. Parametric study

Here, we present a parametric study to investigate the role of model parameters on the ADN-LF consensus protocol. The intricacy of the closed-form expressions for the asymptotic convergence factor — Theorem 3.1 — and its first-order perturbation in the presence of heterogeneity — Theorem 3.2 — might challenge the identification of key parametric dependencies. The latter can be unveiled by exploring the closed-form expressions over a convenient parameter space.

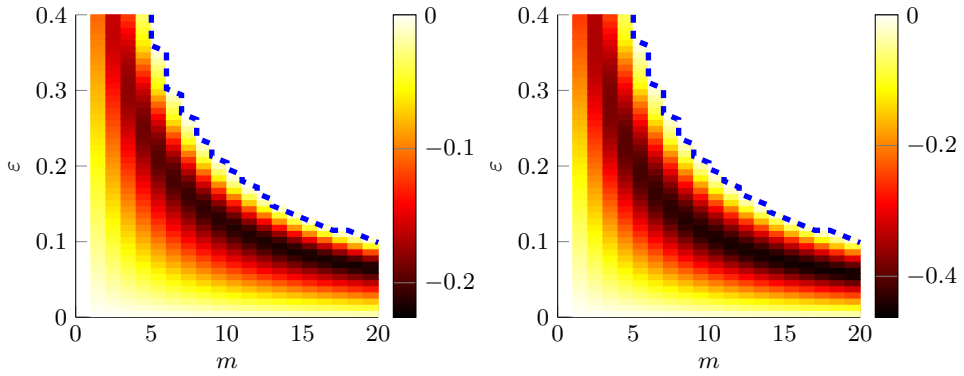

(a) $f = 65$, $a = 0.25$ (b) $f = 50$, $a = 0.4$

Figure 5: Color-coded plot of the logarithm of the asymptotic convergence factor $\log r$ of the ADN-LF consensus as a function of parameters ε and m, for two different choices of the remaining parameters. The blue dashed line identifies the consentability threshold consensus is attained below the threshold). Dark red denotes smaller values of the asymptotic convergence factors, that is, faster convergence toward consensus. In both cases, $\mathbf{a} = a\mathbf{1}$ and $n = 100$.

(a) Homogeneous case

We consider the ADN-LF consensus protocol (2.3) with a homogeneous vector of activities. Proposition 2.1 guarantees mean-square consentability provided that the asymptotic convergence factor is less than one. Since the asymptotic expression of r for large groups, demonstrated in Corollary 3.1, is mostly influenced by the averaging parameter ε and the number of connections m, we begin our analysis with these two parameters.

Fig. 5 summarizes this parameter exploration. We color-code the regions of the parameter space where the system is mean-square consentable, according to the $\log r$. Above the dashed line, associated with $r = 1$, mean-square consensus is not feasible. The number of connections that are formed by each node plays a key role on consentability. Within the consentable region, we can identify optimal combinations of ε and m that maximize the speed of convergence. The shape of the optimality locus highlights a trade-off between the tendency to compromise and the number of interactions established at each time-step: if one increases, the other should decrease, and vice versa. A similar trade-off has been recently documented and investigated in an experimental setup using a swarm of land robots [60].

In Fig. 6, we extend the analysis to the fraction of followers $\kappa = f/n$ and the activity a by examining pair-wise variations of κ, a, and ε. Predictably, Fig. 6a shows that the asymptotic convergence factor improves by increasing the number of leaders, consistent with the empirical observations on the advantageous role of leaders for the group in [12–14]. Given the fraction of leaders, we identify an optimal value for the averaging parameter ε, such that higher or lower values of ε reduce the convergence rate, potentially causing consentability to be lost. Fig. 6b shows that the convergence rate improves with the activity of the nodes, since higher values of a are more conducive to information exchange in the group. Also in this case, for any given value of a, we determine an optimal value of ε that maximizes the convergence rate. Finally, in Fig. 6c, we demonstrate that the rate of convergence rate improves monotonically with both the activity and the fraction of leaders.

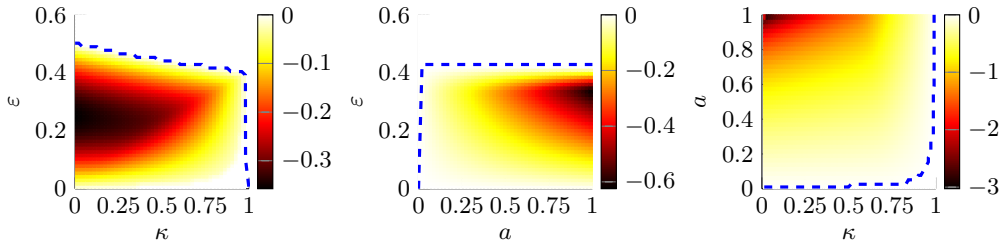

(a) $a = 0.3$ (b) $f = 80$ (c) $\varepsilon = 0.3$

Figure 6: Color-coded plot of the logarithm of the asymptotic convergence factor $\log r$ of the ADN-LF consensus protocol, as a function of ε, κ, and a, for two different choices of the remaining parameters. The blue dashed line identifies the consentability threshold (consensus is attained below the threshold for (a) and (b), while it is reached above the threshold for (c)). Common parameters are $n = 100$ and $m = 4$.

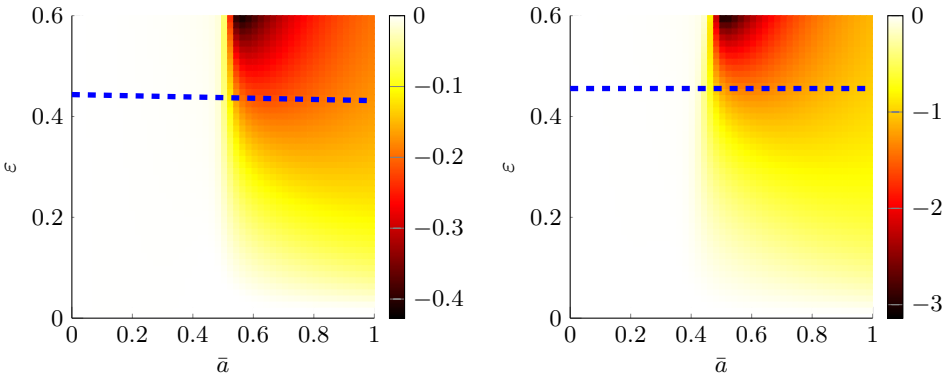

(a) $f = 65, \sigma = 0.2$ (b) $f = 50, \sigma = 0.35$

Figure 7: Color-coded plot of the effect of heterogeneity in the nodes' activities on the asymptotic the convergence factor of an ADN-LF, as a function of ε and $\bar{a}$. The blue dashed line identifies the consentability threshold for nodes with the same activity, that is, $\sigma = 0$ (consensus is possible above the threshold). Common parameters are $n = 100$, $m = 4$, and $\alpha = 1$.

(b) Heterogeneous case

We consider now the general case in which the activities of the agents are different. In Fig. 7, we examine the effect of heterogeneity in the activities by computing the ratio $\sigma\rho_1/\lambda_6$, quantifying the relative difference between the spectral radii of H and H_0 up to the first-order in σ, according to Theorem 3.2. We examine variations in ε and $\bar{a}$. For low levels of the average activity $\bar{a}$, the performance of the ADN-LF consensus protocol is not sensibly affected by heterogeneity, whereby the relative difference between the spectral radii is close to zero. As the average activity grows, that is, for increasing values of $\bar{a}$, we observe a robust improvement in the convergence rate. We acknowledge that our analysis is limited to a first-order perturbation, whereby the location of the stability boundary for $\sigma > 0$ can only be identified for moderately heterogeneously systems. For sufficiently large values of the averaging parameter ε, we observe a nonmonotonic dependence on bar a. This supports the existence of an optimal value of average activity $\bar{a}$, yielding the largest improvement in the speed of convergence.

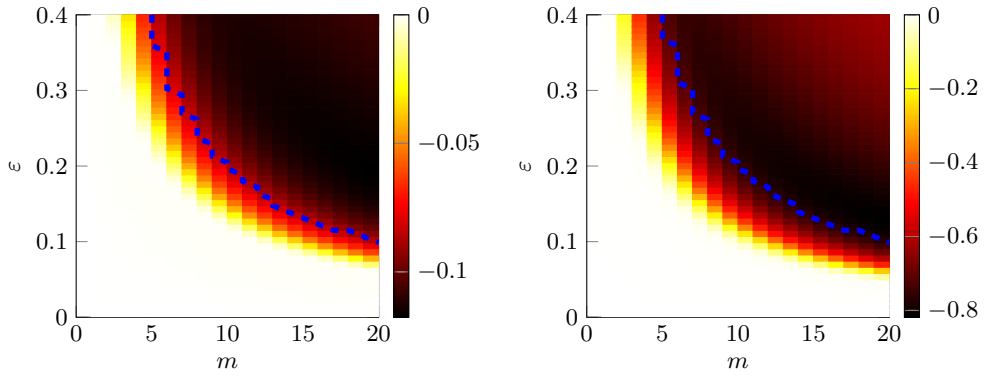

(a) $f = 65, \bar{a} = 0.25$, and $\sigma = 0.2$ (b) $f = 50, \bar{a} = 0.4$, and $\sigma = 0.35$

Figure 8: Color-coded plot of the effect of heterogeneity in the nodes' activities on the asymptotic the convergence factor of an ADN-LF, as a function of σ, ε, and $\bar{a}$. The blue dashed line identifies the consentability threshold for nodes with the same activity, that is, $\sigma = 0$ (consensus is possible above the threshold). Common parameters are $n = 100$ and $\alpha = 1$.

Recalling the role of the trade-off between ε and m on the convergence rate for the case of homogeneous activities demonstrated in Fig 5, we explore the mediating effect of heterogeneous activities. In Fig. 8, we plot $\sigma\rho_1/\lambda_6$ as a function of ε and m for two exemplary values of σ. Therein, we identify a wide region of the parameter space for which heterogeneity in activities dramatically improves the convergence of the consensus protocol. Improvement is registered in terms of faster convergence rates as well as a wider parameter space in which consensus should be feasible, echoing experimental evidence that supports a potential benefit of heterogeneity in behavioral and non-behavioral traits in social groups [48–51].

5. Conclusions

In this work, we have studied the problem of stochastic leader-follower consensus in a multi-agent system encapsulating some of the critical aspects of social groups. We have framed our model within the paradigm of activity-driven networks, which allows for incorporating the stochastic nature of interactions between group members, perceptual limitations of individuals, and heterogeneity in individual tendency to share information in the group. Our main contributions are: (i) the formalization of a leader-follower consensus protocol over an activity-driven network; (ii) the analytical computation of the second moment matrix of such a protocol, whose spectral radius regulates the rate of convergence to consensus; (iii) the rigorous computation of a closed-form expression for the convergence rate of the protocol when all individuals have the same activity; and (iv) the application of eigenvalue perturbation techniques toward a closed-form result that helps elucidate the effect of the heterogeneity in individuals' activity on the convergence rate.

Although many features can be utilized to measure the performance of collective behavior [15, 61], we focused on the convergence rate, which bears important ramifications on animal and human groups. For instance, fish that have the ability to rapidly coordinate among each other through local decision-making form large schools with improved foraging success [62,63]. Expanding to human teams, increased convergence rate could beget faster decision-making in social communities [64,65].

Interestingly, our analytical results share similarities with observed traits of animal and human groups, whereby we found that heterogeneity in individual activities could favor consensus. Several biological observations indicate that heterogeneity in behavioral and non-behavioral traits

can be beneficial to coordination and performance in social groups [48–53]. For example, spiders achieve advantages in terms of nest defense, foraging, or parental care, when their communities are populated by heterogeneous phenotypes, and heterogeneous bee colonies have enhanced productivity and fitness [51]. Likewise, human teams of workers benefit from heterogeneity in terms of increased performance in banks and industrial firms [52,53]. Our study adds to this field of investigation by demonstrating that the convergence rate of a class of stochastic leader-follower consensus protocols can be improved by engineering the extent of heterogeneity in the system.

While in many real-world applications it is tenable to assume that leaders share a common state (for instance, due to precursory dynamics or the presence of an external controller), other scenarios may call for the inclusion of a some level of disagreements among the leaders. From a technical point of view, such an extension would yield a different structure of the second moment matrix. As a result, the problem could not be directly treated with the techniques presented in this paper. However, we believe that a similar perturbation argument can be put forward, shedding light on the role of heterogeneity within the leaders subset.

Another limitation of our study resides in the perturbation argument used to deal with the heterogeneous scenario. Despite numerical simulations suggest that the first-order approximation is accurate for perturbations up to the same order of magnitude of the average value of the activity, a higher-order perturbation analysis would be necessary to extend our results to highly heterogeneous systems. The implementation of such an analysis will be part of our future research. While in many real-world applications it is tenable to assume that leaders share a common state (for instance, due to precursory dynamics or the presence of an external controller), other scenarios may call for the inclusion of a some level of disagreements among the leaders. From a technical point of view, such an extension would yield a different structure of the second moment matrix. As a result, the problem could not be directly treated with the techniques presented in this paper. However, we believe that a similar perturbation argument can be put forward, shedding light on the role of heterogeneity within the leaders subset. Besides, other avenues of future research include the extension of this approach to nonlinear dynamics, which can be implemented by formulating a master stability equation [66], and the analysis of experimental case-studies to examine the viability of control strategies for collective behavior of social groups based on the targeted introduction of heterogeneity.

Data Accessibility. The codes used to produce the figures are available at `https://gitlab.com/PoliToComplexSystemLab/adnlf.git`.

Authors' Contributions. MP and AR designed and supervised the research. JH and LZ performed the mathematical derivations and numerical simulations. DBL, JH, and LZ wrote a first, preliminary draft of the manuscript. MP and AR wrote the initial submission of the manuscript. MP, AR, and LZ revised the manuscript based on the comments of the anonymous reviewers and prepared the final version of the work. All the authors edited and commented the final version.

Competing Interests. We declare we have no competing interests.

Funding. This work was partially supported by the National Science Foundation under grant number CMMI-1561134; the Compagnia di San Paolo, Torino, Italy; and the Italian Ministry of Foreign Affairs and International Cooperation under grant "Mac2Mic".

Acknowledgements. LZ acknowledges the support from the Faculty of Science and Engineering, University of Groningen, Groningen, The Netherlands, which is his current affiliation.

Appendix

Coefficients in the formulations of eigenvalues and eigenspaces

The coefficients that appear in Proposition 3.2 are calculated as

$$\gamma_{3,4} = \frac{-B_\gamma \pm \sqrt{B_\gamma^2 - 4A_\gamma C_\gamma}}{2A_\gamma}, \qquad \gamma_{5,6} = \frac{-\widehat{B}_\gamma \pm \sqrt{\widehat{B}_\gamma^2 - 4\widehat{A}_\gamma \widehat{C}_\gamma}}{2\widehat{A}_\gamma}, \tag{A 1}$$

with

$$\begin{aligned}
A_\gamma &= 1-nqa,\\
B_\gamma &= (4-f)(1-nqa)+q(1-a)(n-1)^2+qa-\varepsilon,\\
C_\gamma &= 2(f-2)\left[nqa-1+2q(1-a)n+\frac{q-\varepsilon}{n-2}\right],\\
\widehat{A}_\gamma &= \varepsilon(f-1)+\varepsilon\frac{(m-1)(f-1)(f-2)}{n-2}+q(n-1)(\ell-f+1)-qa\ell^2,\\
\widehat{B}_\gamma &= \varepsilon(f-1)-2f+q(n-1)^2+qa(n+\ell-\ell^2),\\
\widehat{C}_\gamma &= qa(n+\ell)-2.
\end{aligned} \tag{A 2}$$

The coefficients $\omega_3,\dots,\omega_6$ that appear in Theorem 3.1 are computed by evaluating the right-hand-sides of (A 1), with the coefficients that have γ as a subscript being replaced by the following ones:

$$\begin{aligned}
A_\omega &= qan-q(n-1)-\varepsilon\frac{m-1}{n-2},\\
B_\omega &= -qan(n-2)+q(n^2-3n+1)1-\varepsilon,\\
C_\omega &= 2(1-qan),\\
\widehat{A}_\omega &= q^2a(n-1)-q^2a^2n^2+(f-1)q\varepsilon a-qa\varepsilon\frac{(f-2)(m-2)}{n-2},\\
\widehat{B}_\omega &= 1-qa(2f-(f-1)\varepsilon)+3q^2a(n-1)-(n^2+f^2+2\ell-f)q^2a^2-2qa\varepsilon\frac{(f-2)(m-2)}{n-2},\\
\widehat{C}_\omega &= -2qa-qa\varepsilon\frac{(f-2)(m-2)}{n-2}-2q^2a^2(n-1)+2q^2a(n-1).
\end{aligned} \tag{A 3}$$

Proofs of the technical propositions

Proof of Proposition 3.2. We recall that $\mathbf{v}$ is an eigenvector of H associated with the eigenvalue λ if and only if the following relation is verified:

$$(H\mathbf{v})_i=\sum_{j\in\mathcal{F}}H^{ij}\mathbf{v}_j=H^{ii}\mathbf{v}_i+\sum_{j\in\mathcal{F}\setminus\{i\}}H^{ij}\mathbf{v}_j=\lambda(H\mathbf{v})_i,\qquad\forall\, i\in\mathcal{F}. \tag{A 4}$$

Using (A 4), we verify that the quantities expressed in (3.7) and (3.6) are the six pairs of eigenvalues and eigenspaces of H, respectively. To simplify the notation, all the summations in the following should be intended over the set $\mathcal{F}$.

Let us consider a generic vector $\mathbf{v}\in\Gamma_1$. We observe that $\mathbf{v}_i^T\mathbf{1}=0$, $\mathbf{e}_i^T\mathbf{v}_i=0$, and $\sum\mathbf{v}_i=0$. This gives $(H\mathbf{v})_i=\lambda_1\mathbf{v}_i$, that is, λ_1 is an eigenvalue of H with eigenspace Γ_1. Its (geometric) multiplicity is computed by counting the number or linearly independent vectors in Γ_1, which is equal to f^2-3f+1.

For $\mathbf{v}\in\Gamma_2$, the following relationships hold: $\mathbf{v}_i^T\mathbf{1}=-f\mu_i$, $\mathbf{e}_i^T\mathbf{v}_i=0$, $\sum\mathbf{v}_i=f\sum\mu_j\mathbf{e}_j$, and $\mathbf{e}_i^T\mathbf{v}_j=\mu_i-\mu_j$, for $j\neq i$. Hence, $(H\mathbf{v})_i$ reduces into a linear combination of $-\mu_i\mathbf{1}$ and $\sum\mu_j\mathbf{e}_j$, both with weights equal to λ_2, which yields the second eigenvalues. Its multiplicity is equal to $f-1$.

We consider a generic vector in the form $\mathbf{v}=[\mathbf{v}_1^T\dots\mathbf{v}_f^T]^T$, with

$$\mathbf{v}_i=\mu_i\mathbf{e}_i-\frac{1}{\gamma+2}\left(\mu_i\mathbf{1}+\sum_{j\in\mathcal{F}}\mu_j\mathbf{e}_j\right),\quad\sum_{j\in\mathcal{F}}\mu_j=0,\quad i\in\mathcal{F} \tag{A 5}$$

for some $\gamma\in\mathbb{R}\setminus\{2\}$, and we demonstrate that $\mathbf{v}$ is an eigenvector of H_0 if and only if $\gamma=\gamma_3$ or $\gamma=\gamma_4$, with eigenvalues λ_3 and λ_4, respectively. We observe that $\mathbf{v}_i^T\mathbf{1}=\mu_i(\gamma-f+2)/(\gamma+2)$, $\mathbf{e}_i^T\mathbf{v}_i=\mu_i\gamma/(\gamma+2)$, $\sum\mathbf{v}_i=(\gamma-f+2)/(\gamma+2)\sum\mu_j\mathbf{e}_j$, and $\mathbf{e}_i^T\mathbf{v}_i=-(\mu_i+\mu_j)/(\gamma+2)$, for $j\neq i$. Using these properties, we write $(H\mathbf{v})_i$ as a linear combination of $\mu_i\mathbf{e}_i$, $\mu_i\mathbf{1}$, and $\sum\mu_j\mathbf{e}_j$, whose coefficients are first-order polynomials in γ and are denoted as K_1 for the first term and K_2 for the other two terms, respectively. Then, we determine the values of γ for which $\mathbf{v}$ is an eigenvector, by using (A 4). We derive the condition $K_2/K_1=-1/(\gamma+2)$, which yields the second-order

equation $A_\gamma\gamma^2 + B_\gamma\gamma + C = 0$, whose solutions are $\gamma_{3,4}$. Finally, by substituting these two values in (A 4), we obtain $(H\mathbf{v})_i = \lambda_{3,4}\mathbf{v}_i$, which yields the third and the fourth pairs of eigenvalues and eigenspaces. Both eigenspaces have dimension $f-1$.

Lastly, similar to the previous case, we consider a generic vector in the form $\mathbf{v} = [\mathbf{v}_1^T \dots \mathbf{v}_f^T]^T$, with $\mathbf{v}_i = \mathbf{e}_i + \gamma\mathbf{1}$, for $i \in \mathcal{F}$ and for some $\gamma \in \mathbb{R}$, and we prove that $\mathbf{v}$ is an eigenvector if and only if $\gamma = \gamma_5$ or $\gamma = \gamma_6$, with eigenvalues λ_5 and λ_6, respectively. We observe that $\mathbf{v}_i^T\mathbf{1} = 1 + \gamma f$, $\sum \mathbf{v}_i = (1+\gamma f)\mathbf{1}$, and $\mathbf{e}_i^T\mathbf{v}_i = 1+\gamma$, $\mathbf{e}_i^T\mathbf{v}_j = \gamma$ for $i \neq j$. Similar to the previous case, the explicit computation of the product $(H\mathbf{v})_i$ yields a linear combination of $\mathbf{e}_i$ and $\mathbf{1}$, whose coefficients, denoted as K_1' and K_2', respectively, are first-order polynomials in γ. From (A 4), we derive the condition $K_2'/K_1' = \gamma$, which yields the second-order equation $\tilde{A}_\gamma\gamma^2 + \tilde{B}_\gamma\gamma + \tilde{C} = 0$, whose solutions are $\gamma_{5,6}$. Finally, we substitute these two values in (A 4), obtaining λ_5 and λ_6, which are both simple eigenvalues.

We conclude the proof by observing that all the eigenspaces are mutually orthogonal, which can be proved by directly computing the scalar products of pairs of eigenvalues and using again the properties above. Also, the sum of the geometric multiplicities of the eigenvalues is equal to the dimension of H, which implies that all $\lambda_1, \dots, \lambda_6$ are all the (right) eigenvalues of H and that the matrix is diagonalizable [67]. □

Computation of the left eigenspaces of H_0 in Theorem 3.1. Left eigenspaces $\Omega_1, \dots, \Omega_6$ are computed similar to the right ones, following the proof of Proposition 3.2 and using the fact that they share the same eigenvalues. In particular, we obtain that λ_1 and λ_2 have the same left and right eigenspaces, that is, $\Omega_1 = \Gamma_1$ and $\Omega_2 = \Gamma_2$, respectively. As the other eigenspaces are considered, we prove that $\Omega_{3,4}$ and $\Omega_{5,6}$ share a formally similar structure to $\Gamma_{3,4}$ and $\Gamma_{5,6}$, respectively, where the $\gamma_3, \dots, \gamma_6$ parameters are substituted by $\omega_3, \dots, \omega_6$, computed above. □

Proof of Proposition 3.4. The second moment matrix is expressed in a perturbation form as $H = H_0 + \sigma H_1 + O(\sigma^2)$, where

$$
\begin{aligned}
(H_1)^{ii} \;=\;& \left(\frac{\varepsilon m}{n-1} - \frac{\varepsilon^2 m^2 \bar{a}}{n-1}\right)\left(\mathbf{h}\mathbf{1}^T - h_i\mathbf{e}_i\mathbf{1}^T - \mathrm{diag}\,(\mathbf{h}) + h_i\mathbf{e}_i\mathbf{e}_i^T\right) \\
& - \frac{\varepsilon^2 m^2 \bar{a}}{n-1} h_i\left(\mathbf{1}\mathbf{1}^T - \mathbf{e}_i\mathbf{1}^T - I + \mathbf{e}_i\mathbf{e}_i^T\right) \\
& + \left(\varepsilon^2 m^2 \bar{a} - \varepsilon m\right)\left(\mathrm{diag}\,(\mathbf{h}) + h_i I - 2h_i\mathbf{e}_i\mathbf{e}_i^T\right) \\
& + \left(\varepsilon^2 m^2 - 2\varepsilon m\right) h_i\mathbf{e}_i\mathbf{e}_i^T + \left(\frac{\varepsilon m}{n-1} - \frac{\varepsilon^2 m^2}{n-1}\right) h_i\left(\mathbf{e}_i\mathbf{1}^T - \mathbf{e}_i\mathbf{e}_i^T\right), \\
(H_1)^{ij} \;=\;& \frac{\varepsilon^2 m^2 \bar{a}}{(n-1)^2} h_i\left(\mathbf{1}\mathbf{1}^T - I - \mathbf{e}_i\mathbf{1}^T + \mathbf{e}_i\mathbf{e}_i^T\right) \\
& + \frac{\varepsilon^2 m^2 \bar{a}}{(n-1)^2}\left(\mathbf{h}\mathbf{1}^T - h_i\mathbf{e}_i\mathbf{1}^T - \mathrm{diag}\,(\mathbf{h}) + h_i\mathbf{e}_i\mathbf{e}_i^T\right) + \left(\frac{\varepsilon m}{n-1} - \frac{\varepsilon^2 m^2}{n-1}\right) h_i\mathbf{e}_i\mathbf{e}_i^T \\
& - \frac{\varepsilon^2 m^2 \bar{a}}{n-1}\left(\mathrm{diag}\,(\mathbf{h}) - h_i\mathbf{e}_i\mathbf{e}_i^T\right) + \left(\frac{\varepsilon m}{n-1} - \frac{\varepsilon^2 m^2 \bar{a}}{n-1}\right) h_i\left(I - \mathbf{e}_i\mathbf{e}_i^T\right) \\
& + \frac{\varepsilon^2 m(m-1)}{(n-1)(n-2)} h_i\mathbf{e}_i\left(\mathbf{1} - \mathbf{e}_j - \mathbf{e}_i\right)^T + \frac{\varepsilon^2 m}{N-1} h_i\mathbf{e}_i\mathbf{e}_j^T.
\end{aligned}
\tag{A 6}
$$

From Proposition 3.3, the spectral radius of H can be written as $\rho(H) = \lambda_6 + \sigma\rho_1 + O(\sigma^2)$, where

$$
\rho_1 = \frac{\mathbf{v}^T H_1 \mathbf{v}}{||\mathbf{v}||^2} = \frac{1}{||\mathbf{v}||^2} \sum_{i\in\mathcal{F}} \sum_{j\in\mathcal{F}} \mathbf{v}_i^T (H_1)^{ij} \mathbf{v}_j, \tag{A 7}
$$

with $\mathbf{v} = [\mathbf{v}_1^T, \dots, \mathbf{v}_f^T]^T$, $\mathbf{v}_i = \mathbf{e}_i + \gamma_6\mathbf{1}$, and $||\mathbf{v}|| = \sqrt{\gamma_6^2 f^2 + 2\gamma_6 f + f}$. The vector $\mathbf{v}/||\mathbf{v}||$ is thus the unitary-norm eigenvector associated with the spectral radius of H. The espression in Proposition 3.4 is obtained through cumbersome, but standard, algebra. Specifically, we expand

the summations and the products in (A 7) using (A 6). Then, we simplify them by utilizing the properties of vector $\mathbf{v}$ mentioned in the proof of Proposition 3.2, and further using $\mathbf{v}_i^T\mathbf{h} = h_i + \gamma_6\alpha$. □

References

1. Sumpter, D. J. T., *Collective Animal Behavior*, 1st ed. Princeton, NY, US: Princeton University Press, 2010.
2. Attanasi, A. *et al.*, 2014, Information transfer and behavioural inertia in starling flocks. *Nat. Phys.*, **10**, 691–696, (https://doi.org/10.1038/nphys3035).
3. Ashraf, I., Bradshaw, H., Ha, T.-T., Halloy, J., Godoy-Diana, R., and Thiria, B., 2017, Simple phalanx pattern leads to energy saving in cohesive fish schooling. *Proc. Natl. Acad. Sci. USA*, **114**, 9599–9604, (https://doi.org/10.1073/pnas.1706503114).
4. Ehrlich, P. R. and Levin, S. A., 2005, The evolution of norms. *PLOS Biol.*, **3**, e194, (https://doi.org/10.1371/journal.pbio.0030194).
5. Amato, R., Lacasa, L., Díaz-Guilera, A., and Baronchelli, A., 2018, The dynamics of norm change in the cultural evolution of language. *Proc. Natl. Acad. Sci. USA*, **115**, 8260–8265, (https://doi.org/10.1373/pnas.1721059115).
6. Conradt, L. and Roper, T. J., 2005, Consensus decision making in animals. *Trends Ecol. Evol.*, **20**, 449–456, (https://doi.org/10.1016/j.tree.2005.05.008).
7. Krause, J., Hoare, D., Krause, S., Hemelrijk, C. K., and Rubenstein, D. I., 2000, Leadership in fish shoals. *Fish Fish.*, **1**, 82–89, (10.1111/j.1467-2979.2000.tb00001.x).
8. Nagy, M., Ákos, Z., Biro, D., and Vicsek, T., 2010, Hierarchical group dynamics in pigeon flocks. *Nature*, **464**, 890–893, (https://doi.org/10.1038/nature08891).
9. Dyer, J. R., Johansson, A., Helbing, D., Couzin, I. D., and Krause, J., 2009, Leadership, consensus decision making and collective behaviour in humans. *Philos. Trans. Royal Soc. B*, **364**, 781–789, (https://doi.org/10.1098/rstb.2008.0233).
10. Nakayama, S., Krasner, E., Zino, L., and Porfiri, M., 2019, Social information and spontaneous emergence of leaders in human groups. *J. Royal Soc. Interface*, **16**, 20180938, (https://doi.org/10.1098/rsif.2018.0938).
11. King, A. J., Johnson, D. D., and Van Vugt, M., 2009, The origins and evolution of leadership. *Curr. Biol.*, **19**, R911–R916, (https://doi.org/10.1016/j.cub.2009.07.027).
12. Ballerini, M. *et al.*, 2008, Interaction ruling animal collective behavior depends on topological rather than metric distance: Evidence from a field study. *Proc. Natl. Acad. Sci. USA*, **105**, 1232–1237, (https://doi.org/10.1073/pnas.0711437105).
13. Giardina, I., 2008, Collective behavior in animal groups: theoretical models and empirical studies. *HFSP J.*, **2**, 205–219, (https://doi.org/10.2976/1.2961038).
14. King, A. J., Douglas, C. M., Huchard, E., Isaac, N. J., and Cowlishaw, G., 2008, Dominance and affiliation mediate despotism in a social primate. *Curr. Biol.*, **18**, 1833–1838, (https://doi.org/10.1016/j.cub.2008.10.048).
15. Vicsek, T. and Zafeiris, A., 2012, Collective motion. *Phys. Rep.*, **517**, 71–140, (https://doi.org/10.1016/j.physrep.2012.03.004).
16. Cao, Y., Yu, W., Ren, W., and Chen, G., 2012, An overview of recent progress in the study of distributed multi-agent coordination. *IEEE Trans. Ind. Informat.*, **9**, 427–438, (https://doi.org/10.1109/TII.2012.2219061).
17. Ren, W. and Beard, R. W., *Distributed consensus in multi-vehicle cooperative control*, 1st ed. London, UK: Springer, 2008.
18. Tang, Z.-J., Huang, T.-Z., Shao, J.-L., and Hu, J.-P., 2011, Leader-following consensus for multi-agent systems via sampled-data control. *IET Control Theory A.*, **5**, 1658–1665, (https://doi.org/10.1049/iet-cta.2010.0653).
19. Cao, W., Zhang, J., and Ren, W., 2015, Leader-follower consensus of linear multi-agent systems with unknown external disturbances. *Syst. Control Lett.*, **82**, 64–70, (https://doi.org/10.1016/j.sysconle.2015.05.007).
20. Defoort, M., Polyakov, A., Demesure, G., Djemai, M., and Veluvolu, K., 2015, Leader-follower fixed-time consensus for multi-agent systems with unknown non-linear inherent dynamics. *IET Control Theory A.*, **9**, 2165–2170, (https://doi.org/10.1049/iet-cta.2014.1301).
21. Babenko, S., Defoort, M., Djemai, M., and Nicaise, S., 2019, Distributed leader-follower consensus for a class of semilinear second-order multiagent systems using time scale theory. *Int. J. Robust Nonlin.*, **29**, 433–450, (https://doi.org/10.1002/rnc.4406).

22. Wu, Y., Wang, Z., Ding, S., and Zhang, H., 2018, Leader-follower consensus of multi-agent systems in directed networks with actuator faults. *Neurocomputing*, **275**, 1177–1185, (https://doi.org/10.1016/j.neucom.2017.09.066).
23. Hong, Y., Hu, J., and Gao, L., 2006, Tracking control for multi-agent consensus with an active leader and variable topology. *Automatica*, **42**, 1177–1182, (https://doi.org/10.1016/j.automatica.2006.02.013).
24. Zhu, W. and Cheng, D., 2010, Leader-following consensus of second-order agents with multiple time-varying delays. *Automatica*, **46**, 1994–1999, (https://doi.org/10.1016/j.automatica.2010.08.003).
25. Bradbury, J. W., Vehrencamp, S. L. *et al.*, *Principles of animal communication*, 2nd ed. Sunderland, MA, US: Sinauer Associates Inc, 1998.
26. Dunbar, R., 1992, Neocortex size as a constraint on group size in primates. *J. Hum. Evol.*, **22**, 469–493, (https://doi.org/10.1016/0047-2484(92)90081-J).
27. Tegeder, R. W. and Krause, J., 1995, Density dependence and numerosity in fright stimulated aggregation behaviour of shoaling fish. *Philos. Trans. Royal Soc. B*, **350**, 381–390, (https://doi.org/10.1098/rstb.1995.0172).
28. Abaid, N. and Porfiri, M., 2010, Fish in a ring: spatiotemporal pattern formation in one-dimensional animal groups. *J. R. Soc. Interface*, **7**, 1441–1453, (https://doi.org/10.1098/rsif.2010.0175).
29. Ma, J., Song, W.-G., Zhang, J., Lo, S.-M., and Liao, G.-X., 2010, k-nearest-neighbor interaction induced self-organized pedestrian counter flow. *Physica A*, **389**, 2101–2117, (https://doi.org/10.1016/j.physa.2010.01.014).
30. Wolf, M. and Weissing, F. J., 2012, Animal personalities: consequences for ecology and evolution. *Trends Ecol. Evol.*, **27**, 452–461, (https://doi.org/10.1016/j.tree.2012.05.001).
31. Killen, S. S., Marras, S., Steffensen, J. F., and McKenzie, D. J., 2011, Aerobic capacity influences the spatial position of individuals within fish schools. *Proc. Royal Soc. B*, **279**, 357–364, (https://doi.org/10.1098/rspb.2011.1006).
32. Abaid, N. and Porfiri, M., 2012, Leader-follower consensus over numerosity-constrained random networks. *Automatica*, **48**, 1845–1851, (https://doi.org/10.1016/j.automatica.2012.05.058).
33. Roy, S. and Abaid, N., 2016, Leader-follower consensus and synchronization in numerosity-constrained networks with dynamic leadership. *Chaos*, **26**, 116309, (https://doi.org/10.1063/1.4967385).
34. Mwaffo, V. and Porfiri, M., 2015, Linear analysis of the vectorial network model in the presence of leaders. *Automatica*, **58**, 160–166, (https://doi.org/10.1016/j.automatica.2015.05.018).
35. Gavrilets, S., Auerbach, J., and Van Vugt, M., 2016, Convergence to consensus in heterogeneous groups and the emergence of informal leadership. *Sci. Rep.*, **6**, 29704, (https://doi.org/10.1038/srep29704).
36. Perra, N., Gonçalves, B., Pastor-Satorras, R., and Vespignani, A., 2012, Activity driven modeling of time varying networks. *Sci. Rep.*, **2**, 469, (https://doi.org/10.1038/srep00469).
37. Zino, L., Rizzo, A., and Porfiri, M., 2016, Continuous-time discrete-distribution theory for activity-driven networks. *Phys. Rev. Lett.*, **117**, 228302, (https://doi.org/10.1103/PhysRevLett.117.228302).
38. Rizzo, A., Pedalino, B., and Porfiri, M., 2016, A network model for ebola spreading. *J. Theor. Biol.*, **394**, 212–222, (https://doi.org/10.1016/j.jtbi.2016.01.015).
39. Zino, L., Rizzo, A., and Porfiri, M., 2017, An analytical framework for the study of epidemic models on activity driven networks. *J. Complex Net.*, **5**, 924–952, (https://doi.org/10.1093/comnet/cnx056).
40. ——, 2018, Modeling memory effects in activity-driven networks. *SIAM J. Appl. Dyn. Syst.*, **17**, 2830–2854, (https://doi.org/10.1137/18M1171485).
41. Liu, M., Wang, W., Liu, Y., Tang, M., Cai, S., and Zhang, H., 2017, Social contagions on time-varying community networks. *Phys. Rev. E*, **95**, 052306, (https://doi.org/10.1103/PhysRevE.95.052306).
42. Moinet, A., Barrat, A., and Pastor-Satorras, R., 2018, Generalized voterlike model on activity-driven networks with attractiveness. *Phys. Rev. E*, **98**, 022303, (https://doi.org/10.1103/PhysRevE.98.022303).
43. Rizzo, A. and Porfiri, M., 2016, Innovation diffusion on time-varying activity driven networks. *EPJ B*, **89**, 1–8, (https://doi.org/10.1140/epjb/e2015-60933-3).

44. Starnini, M. and Pastor-Satorras, R., 2014, Temporal percolation in activity-driven networks. *Phys. Rev. E*, **89**, 032807, (https://doi.org/10.1103/PhysRevE.89.032807).
45. Kushner, H., *Introduction to stochastic control*, 1st ed. New York, NY,US: Holt, Reinhart, and Winston, 1971.
46. Trefethen, L. and Bau, D., *Numerical Linear Algebra*, 1st ed. Philadelphia, PA, US: SIAM, 1997.
47. Zino, L., Rizzo, A., and Porfiri, M., 2019, Consensus over Activity Driven Networks. *IEEE Trans. Control Netw. Syst.*, (https://doi.org/10.1109/TCNS.2019.2949387).
48. Pruitt, J. N. and Riechert, S. E., 2011, How within-group behavioural variation and task efficiency enhance fitness in a social group. *Proc. Royal Soc. B*, **278**, 1209–1215, (https://doi.org/10.1098/rspb.2010.1700).
49. Pruitt, J. N. and Ferrari, M. C., 2011, Intraspecific trait variants determine the nature of interspecific interactions in a habitat-forming species. *Ecology*, **92**, 1902–1908, (https://doi.org/10.1890/11-0701.1).
50. Wright, C. M., Holbrook, C. T., and Pruitt, J. N., 2014, Animal personality aligns task specialization and task proficiency in a spider society. *Proc. Natl. Acad. Sci. USA*, **111**, 9533–9537, (https://doi.org/10.1073/pnas.1400850111).
51. Mattila, H. R. and Seeley, T. D., 2007, Genetic diversity in honey bee colonies enhances productivity and fitness. *Science*, **317**, 362–364, (https://doi.org/10.1126/science.1143046).
52. Bantel, K. A. and Jackson, S. E., 1989, Top management and innovations in banking: Does the composition of the top team make a difference? *Strategic Manage. J.*, **10**, 107–124, (http://doi.org/10.2307/2486585).
53. Carpenter, M. A. and Fredrickson, J. W., 2001, Top management teams, global strategic posture, and the moderating role of uncertainty. *Acad. Manag. J.*, **44**, 533–545, (http://doi.org/10.2307/3069368).
54. Bollobás, B., *Random graphs*, 2nd ed. Cambridge, UK: Cambridge University Press, 2001.
55. Abaid, N. and Porfiri, M., 2011, Consensus over numerosity-constrained random networks. *IEEE Trans. Autom. Control*, **56**, 649–654, (https://doi.org/10.1109/TAC.2010.2092270).
56. Fang, Y., 1994, Stability analysis of linear control systems with uncertain parameters. Ph.D. dissertation,
57. Fang, Y., Loparo, K. A., and Feng, X., 1995, Stability of discrete time jump linear systems. *J. Math. Syst. Est. Control*, **5**, 275–321.
58. Hibey, J. L., 1996, Stochastic stability theory for systems containing interval matrices. *IEEE Trans. Aerosp. Electron. Syst.*, **32**, 1385–1391, (https://doi.org/10.1109/7.543859).
59. Zhou, J. and Wang, Q., 2009, Convergence speed in distributed consensus over dynamically switching random networks. *Automatica*, **45**, 1455–1461, (https://doi.org/10.1016/j.automatica.2009.01.021).
60. Mateo, D., Horsevad, N., Hassani, V., Chamanbaz, M., and Bouffanais, R., 2019, Optimal network topology for responsive collective behavior. *Sci. Adv.*, **5**, (https://doi.org/10.1126/sciadv.aau0999).
61. De Lellis, P., Polverino, G., Ustuner, G., Abaid, N., Macrì, S., Bollt, E. M., and Porfiri, M., 2014, Collective behaviour across animal species. *Sci. Rep.*, **4**, 3723, (https://doi.org/10.1038/srep03723).
62. Pitcher, T. J., Magurran, A. E., and Winfield, I. J., 1982, Fish in larger shoals find food faster. *Behav. Ecol. Sociobiol.*, **10**, 149–151, (https://doi.org/10.1007/BF00300175).
63. Pitcher, T. J., *The Behaviour of Teleost Fishes*, 1st ed. Boston MA, US: Springer, 1986, 294–337,
64. Eisenhardt, K. M., 1989, Making fast strategic decisions in high-velocity environments. *Acad. Manag. J.*, **32**, 543–576, (https://doi.org/10.2307/256434).
65. Judge, W. Q. and Miller, A., 1991, Antecedents and outcomes of decision speed in different environmental contexts. *Acad. Manag. J.*, **34**, 449–463, (https://doi.org/10.2307/256451).
66. Porfiri, M., 2011, A master stability function for stochastically coupled chaotic maps. *EPL*, **96**, 40014, (https://doi.org/10.1209/0295-5075/96/40014).
67. Bernstein, D. S., *Matrix Mathematics: Theory, Facts, and Formulas*, 2nd ed. Princeton, NJ, US: Princeton University Press, 2011.